

This is the accepted manuscript made available via CHORUS. The article has been published as:

Evolving metric perturbations in dynamical Chern-Simons gravity

Maria Okounkova, Mark A. Scheel, and Saul A. Teukolsky

Phys. Rev. D **99**, 044019 — Published 14 February 2019

DOI: [10.1103/PhysRevD.99.044019](https://doi.org/10.1103/PhysRevD.99.044019)

Evolving Metric Perturbations in dynamical Chern-Simons Gravity

Maria Okounkova* and Mark A. Scheel

*Theoretical Astrophysics, Walter Burke Institute for Theoretical Physics,
California Institute of Technology, Pasadena, CA 91125, USA*

Saul A. Teukolsky

*Theoretical Astrophysics, Walter Burke Institute for Theoretical Physics,
California Institute of Technology, Pasadena, CA 91125, USA and
Center for Astrophysics and Planetary Science, Cornell University, Ithaca, New York 14853, USA*

The stability of rotating black holes in dynamical Chern-Simons gravity (dCS) is an open question. To study this issue, we evolve the leading-order metric perturbation in order-reduced dynamical Chern-Simons gravity. The source is the leading-order dCS scalar field coupled to the spacetime curvature of a rotating black hole background. We use a well-posed, constraint-preserving scheme. We find that the leading-order metric perturbation numerically exhibits linear growth, but that the level of this growth converges to zero with numerical resolution. This analysis shows that spinning black holes in dCS gravity are numerically stable to leading-order perturbations in the metric.

I. INTRODUCTION

Einstein’s theory of general relativity (GR) has passed all precision tests to date and binary black hole observations from the Laser Interferometry Gravitational Wave Observatory (LIGO) have given a roughly 96% agreement with GR [1, 2]. At some scale, however, GR must be reconciled with quantum mechanics in a quantum theory of gravity. Black hole systems can potentially illuminate signatures of quantum gravity, as they probe the strong-field, non-linear, high-curvature regime of gravity.

While several null-hypothesis and parametrized tests of GR with LIGO observations have been performed [2, 3], an open problem is the simulation of binary black holes through full inspiral, merger, and ringdown in a beyond-GR theory. Waveform predictions from such simulations would allow us to perform *model-dependent* tests, and to parametrize the behavior at merger in beyond-GR theories.

From the first LIGO detections, we know that deviations from GR are presently not detectable. It is reasonable to assume that this is because any such deviations are less than about a 4% effect. While it is possible that the signal-to-noise ratio from the merger itself is currently too small to rule out larger deviations at the horizon, we will not consider this possibility here. Accordingly, rather than simulating black holes in a full quantum theory of gravity, we can consider *effective field theories*. These modify the classical Einstein-Hilbert action of GR through the inclusion of classical terms encompassing quantum gravity effects. One such theory is dynamical Chern-Simons (dCS) gravity, which adds a scalar field coupled to spacetime curvature to the Einstein-Hilbert action, and has origins in string theory, loop quantum gravity, and inflation [4–8].

The well-posedness of the initial value problem in full, non-linear dCS gravity is unknown [9]. However, we can work in an *order-reduction scheme*, in which we perturb the dCS scalar field and metric about a GR background. At each order, the equations of motion are well-posed (cf. [10]). In this study, we investigate the behavior of the leading-order dCS metric perturbation, sourced by the leading-order dCS scalar field coupled to the spacetime curvature of a GR background.

The stability of rotating black holes in dCS gravity is unknown [11–13]. In this study, we numerically test the leading-order stability of rotating dCS black holes by evolving the leading-order dCS metric perturbation on a rotating black hole GR background. Since the background (and the leading-order dCS scalar field) are stationary, the dCS metric perturbation should remain stationary if rotating dCS black holes are stable.

This question of stability is of broader importance to our goal of simulating the leading-order dCS metric perturbation of a binary black hole spacetime, in order to produce beyond-GR gravitational waveforms. If rotating black holes in dCS are not stable to leading order, and the metric perturbation grows in time, then we know that we would not be able to simulate black hole binaries in this theory. Specifically, the metric perturbations around each black hole would grow in time during inspiral, and similarly for the final black hole after merger, thus spoiling the evolution.

A. Roadmap and conventions

This paper is organized as follows. In Sec. II, we present the equations of motion of dCS that we aim to evolve in this study. In Sec. III, we derive and present a formalism for stably evolving linear metric perturbations on an arbitrary background, so that we may evolve the leading-order dCS metric perturbation. In Sec. IV, we apply this formalism to evolve the leading-order dCS metric

* mokounko@tapir.caltech.edu

perturbation on a rotating black hole background. We discuss our findings in Sec. V.

We set $G = c = 1$ throughout. Quantities are given in terms of units of M , the ADM mass of the background. Latin letters in the beginning of the alphabet $\{a, b, c, d, \dots\}$ denote 4-dimensional spacetime indices, while Latin letters in the middle of the alphabet $\{i, j, k, l, \dots\}$ denote 3-dimensional spatial indices. g_{ab} refers to the spacetime metric, while γ_{ij} refers to the spatial metric from a 3+1 decomposition with corresponding timelike unit normal one-form n_a (cf. [14] for a review of the 3+1 ADM formalism).

II. DYNAMICAL CHERN-SIMONS GRAVITY

Dynamical Chern-Simons gravity modifies the Einstein-Hilbert action of GR through the inclusion of a scalar field ϑ , coupled to spacetime curvature as

$$S \equiv \int d^4x \sqrt{-g} \left(\frac{m_{\text{pl}}^2}{2} R - \frac{1}{2} (\partial\vartheta)^2 - \frac{m_{\text{pl}}}{8} \ell^2 \vartheta {}^*RR \right). \quad (1)$$

The first term in the action is the familiar Einstein-Hilbert action of general relativity, with the Planck mass denoted by m_{pl} . The second term in the action is a kinetic term for the scalar field. The third term, meanwhile, couples ϑ to spacetime curvature via the Pontryagin density,

$${}^*RR \equiv {}^*R^{abcd} R_{abcd}, \quad (2)$$

where ${}^*R^{abcd} = \frac{1}{2} \epsilon^{abef} R_{ef}{}^{cd}$ is the dual of the Riemann tensor, and $\epsilon^{abcd} \equiv -[abcd]/\sqrt{-g}$ is the fully antisymmetric Levi-Civita tensor. This coupling is governed by a coupling constant ℓ , which has dimensions of length. ℓ physically represents the length scale below which quantum gravity effects become important. One may also include stress-energy terms in this action for additional fields (such as matter terms in a neutron-star spacetime, for example), though we do not write them here.

Varying the dCS action with respect to ϑ gives a sourced wave equation for the scalar field,

$$\square\vartheta = \frac{m_{\text{pl}}}{8} \ell^2 {}^*RR, \quad (3)$$

where $\square = \nabla_a \nabla^a$ is the d'Alembertian operator. Varying the action with respect to the metric g_{ab} gives

$$m_{\text{pl}}^2 G_{ab} + m_{\text{pl}} \ell^2 C_{ab} = T_{ab}^\vartheta, \quad (4)$$

where

$$C_{ab} \equiv \epsilon_{cde(a} \nabla^d R_{b)}{}^c \nabla^e \vartheta + {}^*R^c{}_{(ab)}{}^d \nabla_c \nabla_d \vartheta, \quad (5)$$

and T_{ab}^ϑ is the stress energy tensor for a canonical, massless Klein-Gordon field

$$T_{ab}^\vartheta = \nabla_a \vartheta \nabla_b \vartheta - \frac{1}{2} g_{ab} \nabla_c \vartheta \nabla^c \vartheta. \quad (6)$$

It is the inclusion of C_{ab} in Eq. (4) that modifies the equation of motion for the metric from that of a metric in GR sourced by a scalar field.

C_{ab} , as given in Eq. (5), contains third derivatives of the metric, thus modifying the principal part of the equation of motion for γ_{ab} from that of GR. Because of the presence of these third-derivative terms, it is unknown whether dCS has a well-posed initial value formulation [9].

However, one can expand the scalar field and metric about a GR background as

$$g_{ab} = g_{ab}^0 + \sum_{k=1}^{\infty} \varepsilon^k h_{ab}^{(k)}, \quad (7)$$

$$\vartheta = \sum_{k=0}^{\infty} \varepsilon^k \vartheta^{(k)}, \quad (8)$$

where ε is an order-counting parameter. At each order in ε one recovers an equation of motion with the same principal part as GR. This is known as an *order-reduction scheme*, and has been previously implemented in [10] and [15].

In this scheme, ε^0 simply gives the Einstein field equations of general relativity for $g_{ab}^{(0)}$, with no source term for $\vartheta^{(0)}$, which we can thus set to zero. At first order, we obtain a wave equation for the leading-order scalar field,

$$\square^{(0)} \vartheta^{(1)} = {}^*RR^{(0)}, \quad (9)$$

where $\square^{(0)}$ is the d'Alembertian operator of the background, and ${}^*RR^{(0)}$ is the Pontryagin density of the background. At this order, the metric perturbation $h_{ab}^{(1)}$ is unsourced, and thus we set it to zero. At order ε^2 , the metric perturbation $h_{ab}^{(2)}$ is sourced by the leading-order scalar field $\vartheta^{(1)}$ coupled to spacetime curvature as

$$m_{\text{pl}}^2 G_{ab}^{(0)} [h_{ab}^{(2)}] = -m_{\text{pl}} \ell^2 C_{ab}^{(1)} \vartheta^{(1)} + \frac{1}{8} T_{ab}^{(\vartheta^{(1)})}, \quad (10)$$

where $G_{ab}^{(0)}$ is the Einstein field equation operator of the background, and

$$T_{ab}^{(\vartheta^{(1)})} \equiv \nabla_a^{(0)} \vartheta^{(1)} \nabla_b^{(0)} \vartheta^{(1)} - \frac{1}{2} g_{ab}^{(0)} \nabla_c^{(0)} \vartheta^{(1)} \nabla^{c(0)} \vartheta^{(1)}, \quad (11)$$

where $\nabla_a^{(0)}$ denotes the covariant derivative associated with $g_{ab}^{(0)}$. Meanwhile,

$$C_{ab}^{(1)} \equiv \epsilon_{cde(a} \nabla^{d(0)} R_{b)}{}^c \nabla^{e(0)} \vartheta^{(1)} + {}^*R^c{}_{(ab)}{}^d \nabla_c^{(0)} \nabla_d^{(0)} \vartheta^{(1)}. \quad (12)$$

Note that though $C_{ab}^{(1)}$ contains third derivatives of the background metric $g_{ab}^{(0)}$, it does not contain derivatives of $h_{ab}^{(2)}$, and hence does not contribute to the principal part of Eq. (10). We can thus write the RHS of Eq. (10) in terms of an effective stress energy tensor,

$$T_{ab}^{\text{eff}(1)} \equiv -m_{\text{pl}} \ell^2 C_{ab}^{(1)} \vartheta^{(1)} + \frac{1}{8} T_{ab}^{(\vartheta^{(1)})}. \quad (13)$$

Let us write Eq. (10) in a more illuminating way, as

$$\begin{aligned} m_{\text{pl}}^2 G_{ab}^{(0)}[h_{ab}^{(2)}] &= \frac{1}{8} T_{ab}^{(\vartheta^{(1)})} \\ &- m_{\text{pl}} \ell^2 \left(\epsilon_{cde(a} \nabla^{d(0)} R_{b)}^{c(0)} \nabla^{e(0)} \vartheta^{(1)} \right. \\ &\left. + {}^* R_{(ab)}^c {}^{d(0)} \nabla_c {}^{(0)} \nabla_d {}^{(0)} \vartheta^{(1)} \right) \vartheta^{(1)}. \end{aligned} \quad (14)$$

As mentioned previously, it is the inclusion of the second term on the right-hand side of Eq. (14) that differentiates the equation of motion for the leading-order metric perturbation in dynamical Chern-Simons theory from that of a simple metric perturbation sourced by a scalar field in general relativity.

Our goal, thus, is to evolve the leading-order metric perturbation $h_{ab}^{(2)}$, sourced by $T_{ab}^{\text{eff}(1)}$. Because this is the leading-order metric perturbation, we only need to work in linear theory. We will thus develop a numerical scheme for stably evolving first-order metric perturbations on an arbitrary GR background with arbitrary source.

From here on, we simplify the notation, writing

$$h_{ab}^{(2)} \equiv \frac{\ell^4}{8} \Delta g_{ab}, \quad \vartheta^{(1)} \equiv \frac{m_{\text{pl}}}{8} \ell^2 \Psi, \quad (15)$$

and thus

$$T_{ab}^{\text{eff}}(\Psi) \equiv -C_{ab}(\Psi) + \frac{1}{8} T_{ab}(\Psi), \quad (16)$$

$$C_{ab}(\Psi) \equiv \epsilon_{cde(a} \nabla^d R_{b)}^{c(0)} \nabla^e \Psi + {}^* R_{(ab)}^c {}^{d(0)} \nabla_c \nabla_d \Psi, \quad (17)$$

$$T_{ab}(\Psi) = \nabla_a \Psi \nabla_b \Psi - \frac{1}{2} g_{ab} \nabla_c \Psi \nabla^c \Psi, \quad (18)$$

with the overall evolution equation

$$G_{ab}^{(1)}[\Delta g_{ab}] = T_{ab}^{\text{eff}}(\Psi). \quad (19)$$

III. EVOLVING METRIC PERTURBATIONS

Our goal now is to outline a formalism to evolve the leading-order metric perturbation in dCS, following Eq. (19). In this section, we derive a more general formalism for evolving leading-order metric perturbations on an arbitrary GR background with arbitrary source, which we will apply to rotating black holes in dCS in Sec. IV.

A. Generalized harmonic formalism

The formalism that we will use to evolve metric perturbations is based on the generalized harmonic formalism [16]. This formulation is a generalization of the well-known harmonic formulation of Einstein's equations, and has seen great success in evolving binary black hole mergers [16–19]. This well-posed formalism involves expressing the gauge freedom in terms of a (nearly) freely specifiable gauge source function

$$H_a = g_{ab} \nabla_c \nabla^c x^b = -\Gamma_a, \quad (20)$$

where $\Gamma_a = g^{bc} \Gamma_{abc}$ for the Christoffel symbol derived from g_{ab} , and ∇_c is the corresponding spacetime covariant derivative. Here, H_a is known as the gauge source function, and is a fixed function of coordinates x^a and g_{ab} (but not derivatives of g_{ab}). In particular, setting $H_a = 0$ corresponds to a harmonic gauge. This framework has seen success in numerical relativity, including the simulation of black hole binaries [18–20].

In this study, we will consider the first-order formulation of the generalized harmonic formalism given in [16]. This involves evolving the spacetime metric g_{ab} , along with variables Π_{ab} and Φ_{iab} corresponding to its time and spatial derivatives defined as

$$\Phi_{iab} \equiv \partial_i g_{ab}, \quad (21)$$

$$\Pi_{ab} \equiv -n^c \partial_c g_{ab}, \quad (22)$$

where n^c is the timelike unit normal vector to slices of constant time t .

For simplicity, we will combine these into a single 4-dimensional variable κ_{abc} , defined as

$$\kappa_{0ab} \equiv \Pi_{ab} = -n^c \partial_c g_{ab}, \quad (23)$$

$$\kappa_{iab} \equiv \Phi_{iab} = \partial_i g_{ab}. \quad (24)$$

Note that κ_{abc} does not obey the tensor transformation law.

In addition to being first order, the formalism given in [16] is also *constraint-damping*. It includes terms proportional to $\partial_i g_{ab} - \kappa_{iab}$, for example; these terms are chosen so that small violations of constraints are driven toward zero. Here, $\partial_i g_{ab}$ is the derivative of g_{ab} taken numerically, while κ_{iab} is the first-order variable corresponding to the spatial derivative of the metric. Terms are added to the evolution equations with (spatially-dependent) multiplicative constants $\gamma_0, \gamma_1, \gamma_2$ to ensure symmetric-hyperbolicity and that the relations in Eqs. (20), (23) and (24) are obeyed.

The first-order, symmetric-hyperbolic, constraint-damping evolution equations for the metric are given by

$$\partial_t g_{ab} = (1 + \gamma_1) \beta^k \partial_k g_{ab} - \alpha \kappa_{0ab} - \gamma_1 \beta^i \kappa_{iab}, \quad (25)$$

$$\begin{aligned} \partial_t \kappa_{iab} &= \beta^k \partial_k \kappa_{iab} - \alpha \partial_i \kappa_{0ab} + \alpha \gamma_2 \partial_i g_{ab} - \alpha \gamma_2 \kappa_{iab} \\ &+ \frac{1}{2} \alpha n^c n^d \kappa_{icd} \kappa_{0ab} + \alpha \gamma^{jk} n^c \kappa_{ijc} \kappa_{kab}, \end{aligned} \quad (26)$$

and

$$\begin{aligned} \partial_t \kappa_{0ab} &= \beta^k \partial_k \kappa_{0ab} - \alpha \gamma^{ki} \partial_k \kappa_{iab} + \gamma_1 \gamma_2 \beta^k \partial_k g_{ab} \\ &+ 2\alpha g^{cd} (\gamma^{ij} \kappa_{ica} \kappa_{jdb} - \kappa_{0ca} \kappa_{0db}) \\ &- g^{ef} \Gamma_{ace} \Gamma_{bdf}) \\ &- 2\alpha \nabla_{(a} H_{b)} - \frac{1}{2} \alpha n^c n^d \kappa_{0cd} \kappa_{0ab} \\ &- \alpha n^c \kappa_{0ci} \gamma^{ij} \kappa_{jab} \\ &+ \alpha \gamma_0 [2\delta^c_{(a} n_{b)} - g_{ab} n^c] (H_c + \Gamma_c) \\ &- \gamma_1 \gamma_2 \beta^i \kappa_{iab} - 2\alpha S_{ab}. \end{aligned} \quad (27)$$

In the last equation, S_{ab} is a source term related to trace-reverse of the stress-energy tensor T_{ab} as

$$S_{ab} = 8\pi(T_{ab} - \frac{1}{2}Tg_{ab}), \quad (28)$$

where $T = g^{ab}T_{ab}$. In the above, $\nabla_a H_b$ is defined as $\partial_a H_b - \Gamma^d_{ab}H_d$, as if H_a were a one-form (which it is not).

B. Linearized generalized harmonic formalism

Our goal in this study is to evolve first-order metric perturbations on a GR background. Given a background $\{g_{ab}, \kappa_{abc}\}$, we perturb it to first order as

$$g_{ab} \rightarrow g_{ab} + \Delta g_{ab}, \quad (29)$$

$$\kappa_{abc} \rightarrow \kappa_{abc} + \Delta \kappa_{abc}. \quad (30)$$

From here on, ΔA will always refer to the linear perturbation to a variable A .

The evolution equations for Δg_{ab} and $\Delta \kappa_{abc}$ can be derived by linearizing Eqs. (25), (26) and (27), and keeping terms to first order. The resulting equations will be a first-order formulation. The symmetric hyperbolicity of these equations is guaranteed because the perturbation equations will have the same principal part as the background system. The linearized system is also constraint damping, as the associated *constraint evolution system* has the same linear part as in the constraint-damping unperturbed system (cf. Eqs. 17 – 21 in [16]). More importantly, the equations for Δg_{ab} and $\Delta \kappa_{abc}$ will have the same principal part as the equations for g_{ab} and κ_{abc} , as we shall see.

Linearizing Eqs. (25), (26) and (27) involves computing terms like $\Delta\alpha$, $\Delta\beta^i$, the first-order perturbations to the lapse and shift. In the following section, we thus derive expressions for these terms in terms of the fundamental variables Δg_{ab} and $\Delta \kappa_{abc}$.

C. Linearized variables

To compute Δg^{ab} , we can use the identity $g^{ab}g_{bc} = \delta^a_c$ to give

$$\Delta g^{ad} = -g^{cd}g^{ab}\Delta g_{bc}. \quad (31)$$

For the perturbation to the lapse, $\Delta\alpha$, the shift, $\Delta\beta^i$, the lower-indexed shift, $\Delta\beta_i$, and the spatial metric $\Delta\gamma_{ij}$ and $\Delta\gamma^{ij}$, we recall that the spacetime metric is decomposed in the 3+1 ADM formalism as

$$g_{ab} = \begin{pmatrix} -\alpha^2 + \beta_i\beta^i & \beta_i \\ \beta_j & \gamma_{ij} \end{pmatrix} \quad (32)$$

$$g^{ab} = \begin{pmatrix} -\alpha^{-2} & \alpha^{-2}\beta^i \\ \alpha^{-2}\beta^j & \gamma^{ij} - \alpha^{-2}\beta^i\beta^j \end{pmatrix}. \quad (33)$$

Recall that spatial quantities are raised and lowered with γ_{ij} , the spatial metric. When we perturb all 10 independent components of g_{ab} , we can find what all of the linearized quantities are in terms of g_{ab} and Δg_{ab} . We begin with perturbing g_{0i} to find $\Delta\beta_i$:

$$\Delta\beta_i = \Delta g_{0i}. \quad (34)$$

Similarly, we can perturb g_{ij} to obtain:

$$\Delta\gamma_{ij} = \Delta g_{ij}. \quad (35)$$

We can now use g^{00} to obtain

$$\Delta\alpha = \frac{1}{2}\alpha^3\Delta g^{00}. \quad (36)$$

Next, using $\gamma^{ij}\gamma_{jk} = \delta^i_k$, we find

$$\Delta\gamma^{im} = -\gamma^{mk}\gamma^{ij}\Delta\gamma_{jk}. \quad (37)$$

From this, we can compute $\Delta\beta^i$ as

$$\Delta\beta^i = \Delta\gamma^{ij}\beta_j + \gamma^{ij}\Delta\beta_j. \quad (38)$$

Finally, we need to compute Δn^a and Δn_a , the perturbed time-like unit normal vector and one-form. We can use the expressions for n^a and n_a in terms of the lapse and shift to obtain the perturbed quantities (cf. [14]). We compute

$$\Delta n_a = (-\Delta\alpha, 0, 0, 0). \quad (39)$$

and

$$\Delta n^a = (-\alpha^{-2}\Delta\alpha, \alpha^{-2}\Delta\alpha\beta^i - \alpha^{-1}\Delta\beta^i). \quad (40)$$

In order to check constraint satisfaction (as will be discussed in Sec. III E), we will also need to obtain the perturbation to γ^b_a . We obtain (cf. Eq. 2.30 in [14]),

$$\Delta\gamma^a_b = \Delta n^a n_b + n^a \Delta n_b. \quad (41)$$

Thus, we have obtained all of the necessary perturbed quantities to perturb the generalized harmonic expressions as well as the constraint expressions that we can obtain from Δg_{ab} . In the next section, we describe the quantities that we can obtain from $\Delta \kappa_{abc}$.

Referring back to Eq. (27), we also need to find expressions for $\Delta\Gamma_{abc}$, the first-order perturbation to the connection compatible with g_{ab} , as well as the first-order perturbation to its trace, $\Delta\Gamma_a$. First, let's compute the perturbation to $\Delta\Gamma_{abc}$. By definition,

$$\Gamma_{abc} = \frac{1}{2}(\partial_b g_{ac} + \partial_c g_{ab} - \partial_a g_{bc}). \quad (42)$$

However, in order to preserve hyperbolicity in the evolution equations, all instances of $\partial_a g_{bc}$ appearing in Γ_{abc} are

replaced with κ_{abc} according to Eqs. (23) and (24) [16], thus giving

$$\Gamma_{abc} = \frac{1}{2} \left((1 - \delta_b^0) \kappa_{bac} + \delta_b^0 (-\alpha \kappa_{0ac} + \beta^i \kappa_{iac}) \right. \\ \left. + (1 - \delta_c^0) \kappa_{cab} + \delta_c^0 (-\alpha \kappa_{0ab} + \beta^i \kappa_{iab}) \right. \\ \left. - (1 - \delta_a^0) \kappa_{abc} - \delta_a^0 (-\alpha \kappa_{0bc} + \beta^i \kappa_{ibc}) \right) \quad (43)$$

where the Kronecker delta symbol δ_b^a picks out the spatial indices $\{1, 2, 3\}$ versus time indices $\{0\}$.

We can perturb Eq. (43) to give

$$\Delta \Gamma_{abc} = \frac{1}{2} \left((1 - \delta_b^0) \Delta \kappa_{bac} \right. \\ \left. + \delta_b^0 (-\Delta \alpha \kappa_{0ac} - \alpha \Delta \kappa_{0ac} + \Delta \beta^i \kappa_{iac} + \beta^i \Delta \kappa_{iac}) \right. \\ \left. + (1 - \delta_c^0) \Delta \kappa_{cab} \right. \\ \left. + \delta_c^0 (-\Delta \alpha \kappa_{0ab} - \alpha \Delta \kappa_{0ab} + \Delta \beta^i \kappa_{iab} + \beta^i \Delta \kappa_{iab}) \right. \\ \left. - (1 - \delta_a^0) \Delta \kappa_{abc} \right. \\ \left. - \delta_a^0 (-\Delta \alpha \kappa_{0bc} - \alpha \Delta \kappa_{0bc} + \Delta \beta^i \kappa_{ibc} + \beta^i \Delta \kappa_{ibc}) \right) \quad (44)$$

Now, for $\Gamma_{bc}^a \equiv g^{ad} \Gamma_{dbc}$, we compute the corresponding perturbations (for future use) via

$$\Delta \Gamma_{bc}^a = \Delta g^{ad} \Gamma_{dbc} + g^{ad} \Delta \Gamma_{dbc}. \quad (45)$$

For the trace of $\Gamma_a \equiv g^{bc} \Gamma_{abc}$, we compute

$$\Delta \Gamma_a = \Delta g^{bc} \Gamma_{abc} + g^{bc} \Delta \Gamma_{abc}, \quad (46)$$

where $\Delta \Gamma_{abc}$ is as above, and Δg^{bc} is given in Eq. (31).

The generalized harmonic gauge source term, H_a , will also have a perturbation, ΔH_a . However, ΔH_a , like H_a , is freely specifiable, with the caveat that it can only depend on g_{ab} and Δg_{ab} but no derivatives of g_{ab} or Δg_{ab} . Throughout this study we will choose a *freezing* gauge condition: we set ΔH_a from the initial data $\Delta H_a = \Delta \Gamma_a(t=0)$, and keep it at this constant value throughout the evolution.

Eq. (27) has a $\nabla_a H_b$ term. Perturbing this quantity, we obtain

$$\Delta(\nabla_a H_b) = \partial_a \Delta H_b - \Delta g^{cd} \Gamma_{dab} H_c \\ - g^{cd} (\Delta \Gamma_{dab} H_c + \Gamma_{dab} \Delta H_c). \quad (47)$$

1. Perturbed initial data

Suppose we are given initial data in the form $\{\Delta g_{ab}, \partial_t \Delta g_{ab}, \partial_i \Delta g_{ab}\}$. Perturbing Eqs. (23) and (24), we can relate $\Delta \kappa_{abc}$ to derivatives of Δg_{ab} :

$$\Delta \kappa_{0ab} = -\Delta n^c \partial_c g_{ab} - n^c \partial_c \Delta g_{ab}, \quad (48)$$

$$\Delta \kappa_{iab} = \partial_i \Delta g_{ab}, \quad (49)$$

where Δn^c is computed from Δg_{ab} using Eq. (40).

2. Source terms

In order to source the metric perturbation, we require a perturbation to the stress energy tensor, ΔT_{ab} . This will appear in the perturbed evolution equations through ΔS_{ab} , the perturbation to S_{ab} defined in Eq. (28), as

$$\Delta S_{ab} = 8\pi (\Delta T_{ab} - \frac{1}{2} (\Delta T g_{ab} + T \Delta g_{ab})), \quad (50)$$

$$\Delta T = \Delta g^{ab} T_{ab} + g^{ab} \Delta T_{ab}. \quad (51)$$

For a vacuum background, we obtain the simpler form

$$\Delta S_{ab} = 8\pi (\Delta T_{ab} - \frac{1}{2} g_{ab} g^{cd} \Delta T_{cd}). \quad (52)$$

D. Perturbed evolution equations

We have now derived the first-order perturbations to all of the variables in Eqs. (25), (26), and (27). We next perturb these equations to linear order, in order to obtain evolution equations for Δg_{ab} and $\Delta \kappa_{abc}$.

We begin by perturbing Eq. (25) to obtain

$$\partial_t \Delta g_{ab} = (1 + \gamma_1) (\Delta \beta^k \partial_k g_{ab} + \beta^k \partial_k \Delta g_{ab}) \\ - \Delta \alpha \kappa_{0ab} - \alpha \Delta \kappa_{0ab} \\ - \gamma_1 \Delta \beta^i \kappa_{iab} - \gamma_1 \beta^i \Delta \kappa_{iab}. \quad (53)$$

Next, we perturb Eq. (26) to give

$$\partial_t \Delta \kappa_{iab} = \Delta \beta^k \partial_k \kappa_{iab} + \beta^k \partial_k \Delta \kappa_{iab} \\ - \Delta \alpha \partial_i \kappa_{0ab} - \alpha \partial_i \Delta \kappa_{0ab} \\ + \Delta \alpha \gamma_2 \partial_i g_{ab} + \alpha \gamma_2 \partial_i \Delta g_{ab} \\ + \frac{1}{2} \Delta \alpha n^c n^d \kappa_{icd} \kappa_{0ab} + \frac{1}{2} \alpha \Delta n^c n^d \kappa_{icd} \kappa_{0ab} \\ + \frac{1}{2} \alpha n^c \Delta n^d \kappa_{icd} \kappa_{0ab} + \frac{1}{2} \alpha n^c n^d \Delta \kappa_{icd} \kappa_{0ab} \\ + \frac{1}{2} \alpha n^c n^d \kappa_{icd} \Delta \kappa_{0ab} \\ + \Delta \alpha \gamma^{jk} n^c \kappa_{ijc} \kappa_{kab} + \alpha \Delta \gamma^{jk} n^c \kappa_{ijc} \kappa_{kab} \\ + \alpha \gamma^{jk} \Delta n^c \kappa_{ijc} \kappa_{kab} + \alpha \gamma^{jk} n^c \Delta \kappa_{ijc} \kappa_{kab} \\ + \alpha \gamma^{jk} n^c \kappa_{ijc} \Delta \kappa_{kab} \\ - \Delta \alpha \gamma_2 \kappa_{iab} - \alpha \gamma_2 \Delta \kappa_{iab}. \quad (54)$$

Finally, we perturb Eq. (27) to obtain

$$\begin{aligned}
\partial_t \Delta \kappa_{0ab} = & \Delta \beta^k \partial_k \kappa_{0ab} + \beta^k \partial_k \Delta \kappa_{0ab} \\
& - \Delta \alpha \gamma^{ki} \partial_k \kappa_{iab} - \alpha \Delta \gamma^{ki} \partial_k \kappa_{iab} \\
& - \alpha \gamma^{ki} \partial_k \Delta \kappa_{iab} \\
& + \gamma_1 \gamma_2 \Delta \beta^k \partial_k g_{ab} + \gamma_1 \gamma_2 \beta^k \partial_k \Delta g_{ab} \\
& + 2 \Delta \alpha g^{cd} (\gamma^{ij} \kappa_{ica} \kappa_{jdb} - \kappa_{0ca} \kappa_{0db} - g^{ef} \Gamma_{ace} \Gamma_{bdf}) \\
& + 2 \alpha \Delta g^{cd} (\gamma^{ij} \kappa_{ica} \kappa_{jdb} - \kappa_{0ca} \kappa_{0db} - g^{ef} \Gamma_{ace} \Gamma_{bdf}) \\
& + 2 \alpha g^{cd} (\Delta \gamma^{ij} \kappa_{ica} \kappa_{jdb} - \Delta \kappa_{0ca} \kappa_{0db} - \Delta g^{ef} \Gamma_{ace} \Gamma_{bdf}) \\
& + 2 \alpha g^{cd} (\gamma^{ij} \Delta \kappa_{ica} \kappa_{jdb} - \kappa_{0ca} \Delta \kappa_{0db} - g^{ef} \Delta \Gamma_{ace} \Gamma_{bdf}) \\
& + 2 \alpha g^{cd} (\gamma^{ij} \kappa_{ica} \Delta \kappa_{jdb} - g^{ef} \Gamma_{ace} \Delta \Gamma_{bdf}) \\
& - 2 \Delta \alpha \nabla_{(a} H_{b)} - 2 \alpha \Delta \nabla_{(a} H_{b)} \\
& - \frac{1}{2} \Delta \alpha n^c n^d \kappa_{0cd} \kappa_{0ab} - \frac{1}{2} \alpha \Delta n^c n^d \kappa_{0cd} \kappa_{0ab} \\
& - \frac{1}{2} \alpha n^c \Delta n^d \kappa_{0cd} \kappa_{0ab} - \frac{1}{2} \alpha n^c n^d \Delta \kappa_{0cd} \kappa_{0ab} \\
& - \frac{1}{2} \alpha n^c n^d \kappa_{0cd} \Delta \kappa_{0ab} \\
& - \Delta \alpha n^c \kappa_{0ci} \gamma^{ij} \kappa_{jab} - \alpha \Delta n^c \kappa_{0ci} \gamma^{ij} \kappa_{jab} \\
& - \alpha n^c \Delta \kappa_{0ci} \gamma^{ij} \kappa_{jab} - \alpha n^c \kappa_{0ci} \Delta \gamma^{ij} \kappa_{jab} \\
& - \alpha n^c \kappa_{0ci} \gamma^{ij} \Delta \kappa_{jab} \\
& + \Delta \alpha \gamma_0 [2\delta^c_{(a} n_{b)} - g_{ab} n^c] (H_c + \Gamma_c) \\
& + \alpha \gamma_0 [2\delta^c_{(a} \Delta n_{b)} - \Delta g_{ab} n^c] (H_c + \Gamma_c) \\
& + \alpha \gamma_0 [-g_{ab} \Delta n^c] (H_c + \Gamma_c) \\
& + \alpha \gamma_0 [2\delta^c_{(a} n_{b)} - g_{ab} n^c] (\Delta H_c + \Delta \Gamma_c) \\
& - \gamma_1 \gamma_2 \Delta \beta^i \kappa_{iab} - \gamma_1 \gamma_2 \beta^i \Delta \kappa_{iab} \\
& - 2 \Delta \alpha S_{ab} - 2 \alpha \Delta S_{ab} .
\end{aligned} \tag{55}$$

E. Constraint Equations

In order to check the numerical performance of the evolution equations given in the previous section, we evaluate a set of four perturbed constraints that Δg_{ab} and $\Delta \kappa_{abc}$ must satisfy. These functions are zero analytically, and we will check their convergence to zero with increasing numerical resolution.

The 1-index constraint (cf. [16]) is the gauge constraint

$$C_a = H_a + \Gamma_a , \tag{56}$$

which measures the numerical accuracy of the generalized harmonic evolution (cf. Eq. (20)). We perturb this to get the constraint

$$\Delta C_a \equiv \Delta H_a + \Delta \Gamma_a , \tag{57}$$

where ΔH_a is the gauge source function for the metric perturbation evolution.

The 3-index constraint evaluates the difference between the numerical derivative of g_{ab} and κ_{iab} , the first-order variable encoding the spatial derivative of the metric as

$$C_{iab} = \partial_i g_{ab} - \kappa_{iab} . \tag{58}$$

Perturbing this, we obtain

$$\Delta C_{iab} = \partial_i \Delta g_{ab} - \Delta \kappa_{iab} . \tag{59}$$

The 4-index constraint concerns the commutation of partial derivatives as

$$C_{ijab} \equiv 2 \partial_{[i} \kappa_{j]ab} . \tag{60}$$

Perturbing this, we obtain

$$\Delta C_{ijab} \equiv 2 \partial_{[i} \Delta \kappa_{j]ab} . \tag{61}$$

Finally, the 2-index constraint is derived from the Hamiltonian and momentum constraints, as well as the 3-index constraint. The constraint and its perturbation are too lengthy to reproduce here, and so we have written them in Appendix A.

Thus, when performing an evolution, we evaluate the right-hand sides of Eqs. (57), (59), (61) and (A6), and check that they converge to zero with increasing numerical resolution. In particular, as we use a spectral code, we expect exponential convergence with resolution [21].

In order to show that the constraints themselves are convergent, rather than the absolute values of the metric variables simply getting smaller, we can normalize the constraints by the absolute values of the metric fields they contain. For example, for a constraint of the form $A + B$, we normalize it by dividing by $\sqrt{A^2 + B^2}$. The question arises of whether we should normalize the constraints pointwise, or whether we should compute the norm of each constraint and its normalization factor over the entire domain and then divide the norms. Since we will evolve a localized metric perturbation, there will be regions in the domain with Δg_{ab} nearly zero, so we choose to first compute norms and then divide them.

F. Characteristic variables

All of the discussion so far has centered on fundamental variables Δg_{ab} and $\Delta \kappa_{abc}$. However, in order to implement boundary conditions, it is useful to instead consider *characteristic fields*. These can be used to measure the characteristic speeds and to construct boundary conditions.

The characteristic fields are the eigenvectors of the principal part of the evolution equations (cf. [16] for an example derivation). The characteristic speeds are the corresponding eigenvalues. For the generalized harmonic system, the characteristic variables on a surface with spatial normal vector \hat{n}^i take the form

$$u_{ab}^0 = g_{ab} , \tag{62}$$

$$u_{ab}^{1\pm} = \kappa_{0ab} \pm \hat{n}^i \kappa_{iab} - \gamma_2 g_{ab} , \tag{63}$$

$$u_{iab}^2 = (\delta_i^k - \hat{n}_i \hat{n}^k) \kappa_{kab} . \tag{64}$$

The principal parts of the linearized equations (cf. Sec III D) are

$$\partial_t \Delta g_{ab} - (1 + \gamma_1) \beta^k \partial_k \Delta g_{ab} \simeq 0, \quad (65)$$

$$\partial_t \Delta \kappa_{0ab} - \beta^k \partial_k \Delta \kappa_{0ab} \quad (66)$$

$$+ \alpha \gamma^{ki} \partial_k \Delta \kappa_{iab} - \gamma_1 \gamma_2 \beta^k \partial_k \Delta g_{ab} \simeq 0,$$

$$\partial_t \Delta \kappa_{iab} - \beta^k \partial_k \Delta \kappa_{iab} \quad (67)$$

$$+ \alpha \partial_i \Delta \kappa_{0ab} - \gamma_2 \alpha \partial_i \Delta g_{ab} \simeq 0.$$

These are exactly those of the generalized harmonic system, and hence the characteristic fields and speeds will be the same. Thus, the characteristic fields of the linearized system are simply

$$\Delta u_{ab}^0 = \Delta g_{ab}, \quad (68)$$

$$\Delta u_{ab}^{1\pm} = \Delta \kappa_{0ab} \pm \hat{n}^i \Delta \kappa_{iab} - \gamma_2 \Delta g_{ab}, \quad (69)$$

$$\Delta u_{iab}^2 = (\delta_i^k - \hat{n}_i \hat{n}^k) \Delta \kappa_{kab}. \quad (70)$$

The reverse transformation from characteristic variables to fundamental variables is then

$$\Delta g_{ab} = \Delta u_{ab}^0, \quad (71)$$

$$\Delta \kappa_{0ab} = \frac{1}{2} (\Delta u_{ab}^{1+} + \Delta u_{ab}^{1-}) + \gamma_2 \Delta u_{ab}^0, \quad (72)$$

$$\Delta \kappa_{iab} = \frac{1}{2} \hat{n}_i (\Delta u_{ab}^{1+} - \Delta u_{ab}^{1-}) + \Delta u_{iab}^2. \quad (73)$$

As in the generalized harmonic system, the characteristic speed for Δu_{ab}^0 is $-(1 + \gamma_1) n_k \beta^k$, the speed for $\Delta u_{ab}^{1\pm}$ is $-n_k \beta^k \pm \alpha$, and the speed for Δu_{iab}^2 is $-n_k \beta^k$.

G. Boundary Conditions

In the previous section, we derived the characteristic fields for the linearized system. In order to complete the evolution system, we must include boundary conditions for these characteristic fields. All of our numerical evolutions include a finite outer boundary, and we choose to use a freezing boundary condition, which sets

$$P(d\Delta u^{(a)}/dt) = 0, \quad (74)$$

where $\Delta u^{(a)}$ is a perturbation to a characteristic field and P refers to the characteristic projection onto the surface. Though more sophisticated conditions are available, especially for computing accurate gravitational radiation (cf. [22–24]), we find that the freezing boundary condition is sufficient for our purposes, especially since the characteristics are initially purely outgoing (out of the computational domain).

When simulating metric perturbations on a spacetime containing one or more black holes, we exclude the region just inside the apparent horizon from the computational domain [25]. This forms a topologically spherical inner boundary. However, there should be no characteristics entering the computational domain from the horizon, and thus we do not need to specify a condition at the inner boundary.

H. Code Tests

Because of the complexity of Eqs. (25), (26), and (27), we perform a series of code tests. These code tests contain no new physics, but rather check that the evolution equations have been implemented correctly. We present the results of these tests in Appendix B.

IV. EVOLVING DCS METRIC PERTURBATIONS

We now apply the formalism given in Sec. III to dynamical Chern-Simons gravity. Specifically, we aim to test the stability of rotating black holes in dCS by evolving the leading-order metric perturbation, Δg_{ab} , governed by Eq. (19), on a rotating black hole background. In GR, this background is given by the Kerr metric. Recall from Eqs. (16), (17), and (18), that it is precisely the inclusion of $C_{ab}(\Psi)$ in the effective stress energy tensor that differentiates dynamical Chern-Simons gravity, where the scalar field is coupled to spacetime curvature via *RR , from a simple metric perturbation sourced by a scalar field in GR.

A. Implementation details

In [15], we derived stationary initial data for Δg_{ab} on a Kerr background sourced by the spacetime curvature of the Kerr background coupled to a stationary field Ψ obeying $\square\Psi = {}^*RR$. [26]. Using these data, we construct $\Delta\kappa_{abc}$ following Eqs. (49) and (48). The source term ΔS_{ab} described in Sec. III C 2 is computed from Ψ using $T_{ab}^{\text{eff}}(\Psi)$ in Eq. (16).

Our computational domain is a set of eleven nested spherical shells, with more shells centered near the horizon and fewer shells further out. The boundary of the innermost shell conforms to the apparent horizon of the background black hole, and the outer boundary is at $R = 200M$. We repeat simulations at three different numerical resolutions determined by a parameter labeled "low", "medium", or "high"; each shell has 5 radial spectral basis points and 6 angular spectral basis points at the lowest resolution, with one more radial and angular basis point added for each increase in our resolution parameter.

We evolve $\{\Delta g_{ab}, \Delta\kappa_{abc}\}$ using the equations in Sec. III D using a spectral code [21]. We apply filtering to the spectral scheme in order to minimize the growth of high-frequency modes [27]. We choose damping parameters γ_0 and γ_2 to be larger close to the horizon, where the metric perturbation is greatest, as shown in Fig. 1. We choose $\gamma_1 = -1$ as in Ref. [16].

B. Results

In Fig. 2, we present the perturbed constraint violation for a spin $\chi = 0.1$ background using the expressions derived in Sec. III E. We see that the constraints remain roughly constant in time, and are exponentially convergent. We check the constraint convergence for every simulation. Note that as we increase the spin, more spectral coefficients are needed to achieve the same level of constraint violation.

In Fig. 3, we present the behavior of the norm of the metric perturbation with time for $\chi = 0.1$ for low, medium,

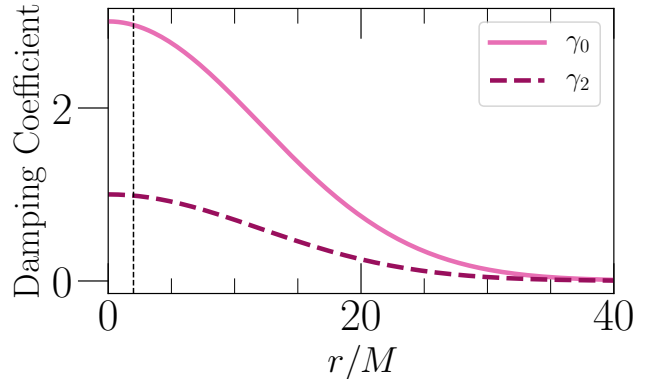


FIG. 1. Constraint damping functions γ_0 and γ_2 used to evolve metric perturbations on a Kerr background. The functions are largest where the metric perturbation source has the highest value, and exponentially decay to $R \rightarrow \infty$. While the functions extend to $R = 0$, the computational domain terminates outside the apparent horizon inner boundary (here shown by the black dashed line at $R = 2M$ in the case of Schwarzschild).

and high resolution. We see that as we increase resolution, Δg_{ab} becomes more constant in time. Note that the specific value of $\|\Delta g_{ab}\|$ (~ 0.86 in Fig. 3) should be a function of χ , the spin of the back hole. However, though expressions for this functional dependence exist in the slow and rapid rotation limits [28, 29], and as post-Newtonian expansions [30], no closed-form, analytical expression for the functional dependence is known.

Fig. 4 similarly shows the behavior of the metric perturbation for $\chi = 0.6$. This case is particularly interesting, as it corresponds roughly to the final spin of the post-merger black holes in [10]. We thus conclude that were we to also simulate metric perturbations in that study, we could stably evolve metric perturbations through ringdown.

For a more quantitative analysis, we show the time derivative of the norm of Δg_{ab} in Figs. 5, 6, and 7, for $\chi = 0.1$, $\chi = 0.6$, and $\chi = 0.9$, for three different resolutions. Initially, there is some junk radiation (unphysical spurious radiation) present on the domain, so the first $\sim 150M$ (corresponding to the computational domain radius) of each figure can be ignored.

We see that after the junk radiation has left the domain, the normalized time derivative decreases with numerical resolution, staying at a low level of $\sim 10^{-6}$ at the highest resolution¹. Let us examine this result more carefully. The metric perturbation, as shown for example in Fig. 3, exhibits linear growth in time. However, the lower numerical resolutions exhibit more linear growth than higher

¹ Higher spins require higher resolutions to achieve the same level of numerical accuracy in Kerr-Schild coordinates, and thus the values of the time derivatives at the same numerical resolution increase slightly with spin.

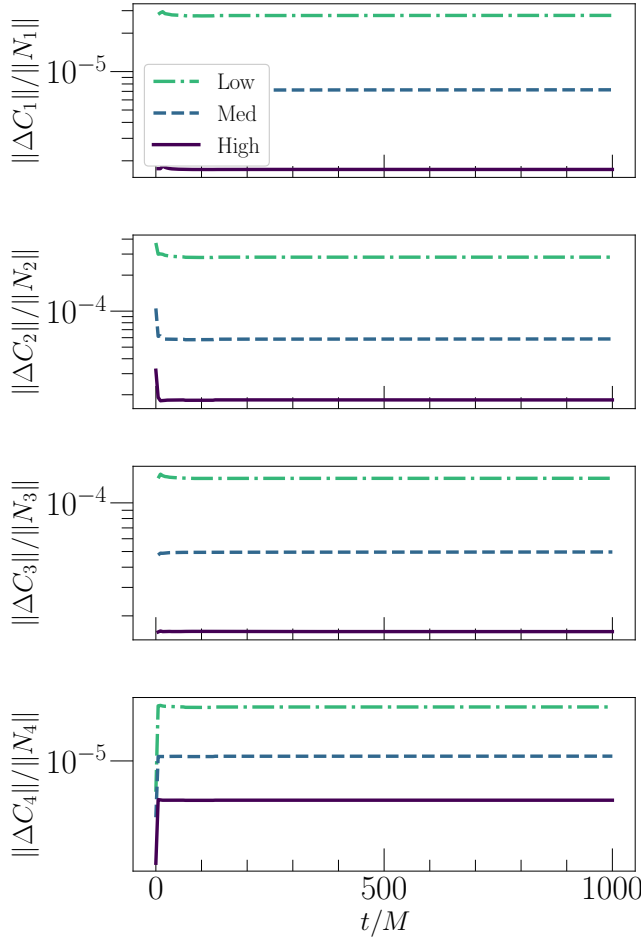


FIG. 2. Behavior of the perturbed constraints given in Sec. III E for a dCS perturbation on a Kerr background with $\chi = 0.1$. For each constraint ΔC_A , we compute the L2 norm of the constraint over the entire computational domain ($\|\Delta C_1\|$ for the 1-index constraint, for example), and divide by the L2 norm of its normalization factor ($\|N_A\|$) (cf. Sec. III E). We see that the constraints remain constant in time and are exponentially convergent with resolution.

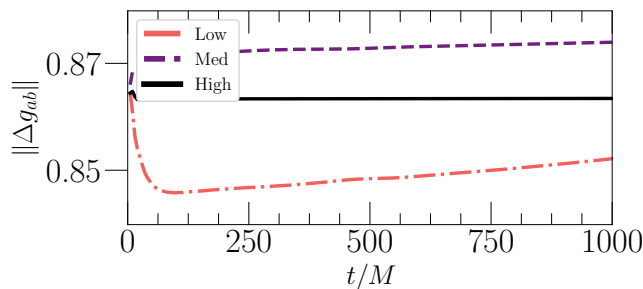


FIG. 3. Metric perturbation Δg_{ab} on a Kerr background with $\chi = 0.1$. We present the behavior at low, medium, and high resolutions, and find that we increase the numerical resolution, the level of linear growth in time decreases.

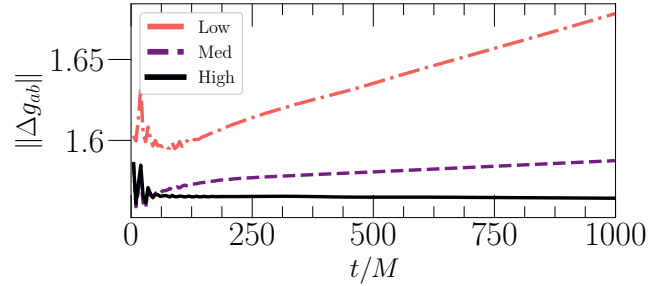


FIG. 4. Similar to Fig. 3, but for spin of $\chi = 0.6$. For each resolution, we use the initial data for Δg_{ab} we have solved for at that resolution, and hence Δg_{ab} has different initial values depending on resolution. We have checked that these initial values converge to the highest-resolution result.

numerical resolutions. As shown in Fig. 5, we see that with increasing numerical resolution, this linear growth converges exponentially towards zero. Thus, this linear growth is a numerical artifact, and in the limit of infinite resolution will be zero. Thus, we must evolve the metric perturbation at a high enough resolution such that the linear growth is small enough for our purposes.

How long do we need to evolve Δg_{ab} to be confident in the stability of the field? Practically, NR gravitational waveforms typically contain 100 – 200 M of ringdown signal [31], as did the simulations we performed in [10]. Thus, we certainly require stability on timescales of $\mathcal{O}(100) M$. Binary black hole simulation initial data is comprised of an approximate superposition of two black hole metrics [32]. Thus, in the early inspiral, the spacetime is similar to that of two black holes, with a dCS metric perturbation isolated around each black hole. While binary black hole simulations typically start $\sim 5,000$ to $10,000 M$ before merger (cf. [31]), at some point in the inspiral, strong-field dynamics take over and the spacetime is no longer a superposition of two Kerr black holes. Thus, we are interested in timescales of $\mathcal{O}(1000) M$, to be able to simulate the early inspiral. For one resolution, we have also evolved Δg_{ab} on a $\chi = 0.1$ background for 10,000 M (but only 1000 M of evolution is shown in Fig. 5). We find that the metric perturbation exhibits similar behavior on these timescales (the time derivative of the perturbed metric, $\partial_t \Delta g_{ab}$, remains at a constant level for at least 10,000 M).

Let us now discuss the origin of the linearly growing mode (a zero-frequency mode). One possibility is that it is present in the initial data for the metric perturbation, as it is in the spectrum of the differential operator. For the simulations shown in Figs. 5, 6, and 7, the evolution for each numerical resolution has its own initial data, which is solved for independently on a grid of that resolution. Thus, if the presence of the mode is purely due to the initial data, we would expect different resolutions to display various levels of linear growth, which we indeed see. To further test this hypothesis, we can instead solve for initial data

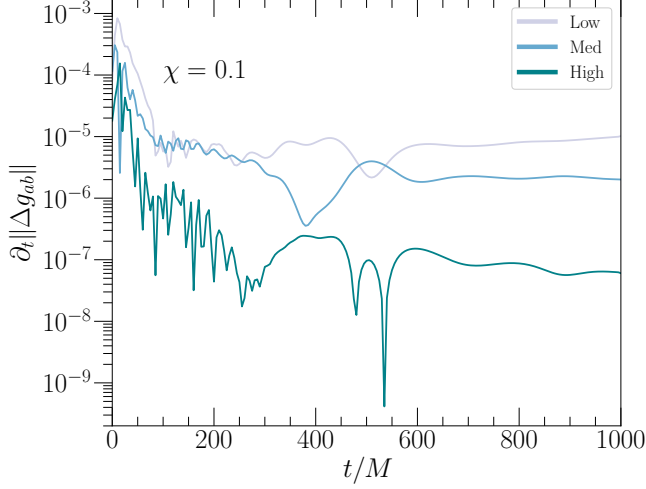


FIG. 5. Behavior of the derivative of the norm of the metric perturbation with time for a background with spin $\chi = 0.1$. We plot $\partial_t \|\Delta g_{ab}\|$, the time derivative of the norm of the metric perturbation. Each line corresponds to a different resolution. We see that after an initial period of junk radiation, the time derivative is convergent towards zero with increasing numerical resolution.

for Δg_{ab} only at the highest resolution, and *interpolate* this onto the lower-resolution grids to use for the evolution. In Fig. 8, we show the results of this procedure. We see that all three resolutions have roughly the same amount of linear growth, suggesting that the zero-frequency mode is seeded by the initial data, rather than spontaneously appearing during the evolution. Note that the growth is at the level of the highest resolution, which is still finite, and hence the growth is non-zero. This in turn tells us that in order to achieve the requisite level of numerical stability, we can use higher-resolution initial data, and perform our simulations at lower resolutions.

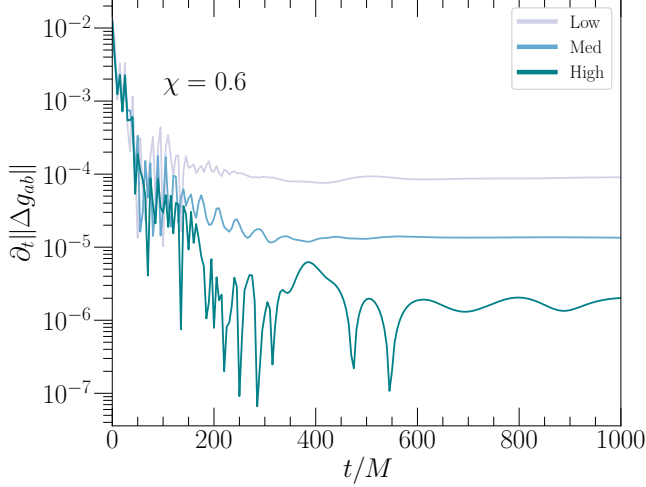


FIG. 6. Similar to Fig. 5, but for spin $\chi = 0.6$.

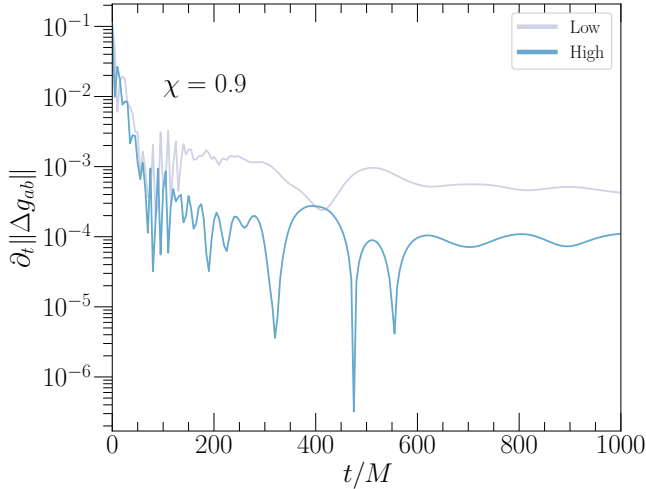


FIG. 7. Similar to Fig. 5, but for spin $\chi = 0.9$.

V. RESULTS AND DISCUSSION

In this paper, we have aimed to test the stability of rotating black holes in dCS gravity to leading order. We have worked in order-reduced dCS, in which we perturb the dCS scalar field and metric around a GR background. We have evolved the leading-order dCS metric perturbation, sourced by the leading-order dCS scalar field coupled to the spacetime curvature of the GR background (Sec. IV). We used a fully general, first-order, constraint-damping metric perturbation evolution scheme based on the generalized harmonic formalism of general relativity (Sec. III). We found that the dCS metric perturbation exhibits linear growth in time, but that the level of linear growth converges towards zero with increasing numerical resolution.

The linear stability analysis presented in this paper

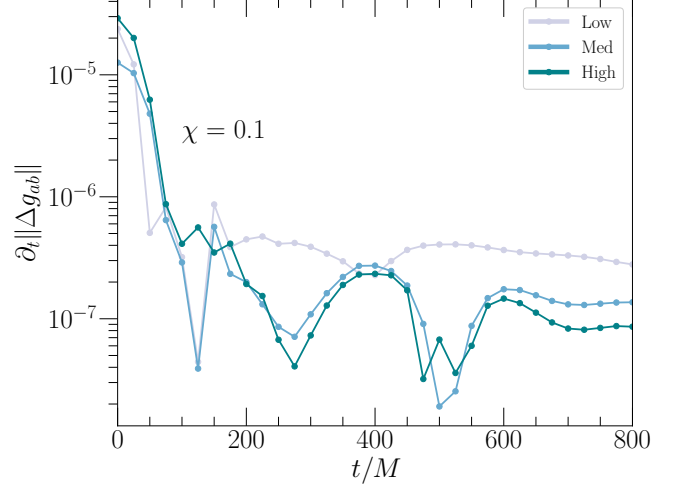


FIG. 8. The structure of this figure is similar to that of Fig. 5. However, in this case, we solve for the initial data for Δg_{ab} purely at the ‘High’ resolution. We interpolate this data onto the ‘Low’ and ‘Medium’ resolution grids to give initial data at these resolutions. We see that as the simulation progresses, the linear growth in Δg_{ab} remains at roughly the same level for all resolutions. This suggests that the zero-frequency mode in Δg_{ab} is present in and due to the resolution of the initial data, rather than spontaneously appearing during the evolution.

shows that black holes in dCS gravity are numerically stable to leading-order perturbations in the metric. The leading-order (first non-vanishing) metric perturbation in dCS gravity occurs at second order, and thus the linear stability presented corresponds to stability at second order in the dCS order-reduction scheme. Previous studies have explored the question of black hole stability in dCS gravity [11–13], but this is the first study to explore the behavior of metric perturbations on a spinning background with non-zero source.

Linear theory has no scale, and thus the results presented in this paper can be applied to any coupling parameter ε^2 such that, to second order, the dCS metric is $g_{ab} + \varepsilon^2 \Delta g_{ab}$. However, for the perturbative scheme to be valid, we must choose ε^2 such that $\|\varepsilon^2 \Delta g_{ab}\| \lesssim \|g_{ab}\|$ (cf. [26] and [15] for a quantitative analysis of allowed values of ε^2).

The stability of our simulations makes us confident that we can evolve dCS metric perturbations in a binary black hole spacetime without numerical instabilities. We can use a superposition of the dCS scalar field initial data given in [26] and the dCS metric perturbation initial data formalism and code used in [15] to generate initial data for scalar field Ψ and perturbed metric variables Δg_{ab} and $\Delta \kappa_{abc}$. We can then evolve the scalar field as we previously have in [10] and use this $\Psi(t)$ to source the evolution of Δg_{ab} . While we have used a stationary gauge as determined by $\Delta H_a = \Delta \Gamma_a(t=0)$ in this work, we also have the option of rolling into a perturbed damped harmonic gauge during the binary evolution (cf. [33]).

ACKNOWLEDGMENTS

We would like to thank Leo Stein for helpful discussions, providing us with the code used to generate the initial data in [26], and careful reading of this manuscript. We would also like to thank Luis Lehner for suggesting this project. This work was supported in part by the Sherman Fairchild Foundation, and NSF grants PHY-1708212 and PHY-1708213 at Caltech and PHY-1606654 at Cornell. Computations were performed using the Spectral Einstein Code [21]. All computations were performed on the Wheeler cluster at Caltech, which is supported by the Sherman Fairchild Foundation and by Caltech.

Appendix A: Perturbed 2-index constraint

In this appendix we derive perturbations to the generalized harmonic constraint C_{ab} . This constraint corresponds to a combination of the Hamiltonian and momentum constraints, and includes terms proportional to the constraint C_{iab} (cf. Eq. (58)) that are added in order to simplify the evolution equations for the constraints [16]. The constraint C_{ab} is defined in Eqs. 43 and 44 of [16], in which the time components C_{0a} are called \mathcal{F}_a . The expressions in [16] do not contain stress-energy source terms, but we include these terms here. In particular,

$$C_{0a} \equiv \mathcal{F}_a - 2n^b S_{ba} + n_a S_{bc} g^{bc}, \quad (\text{A1})$$

where \mathcal{F}_a is the expression from [16].

In terms of the variable κ_{abc} , the spatial part of the

2-index constraint is

$$\begin{aligned} C_{ia} \equiv & \gamma^{jk} \partial_j \kappa_{ika} - \frac{1}{2} \gamma^j{}_a g^{cd} \partial_j \kappa_{icd} + n^b \partial_i \kappa_{0ba} \\ & - \frac{1}{2} n_a g^{cd} \partial_i \kappa_{0cd} + \partial_i H_a + \frac{1}{2} g^j{}_a \kappa_{jcd} \kappa_{ie f} g^{ce} g^{df} \\ & + \frac{1}{2} \gamma^{jk} \kappa_{jcd} \kappa_{ike} g^{cd} n^e n_a \\ & - \gamma^{jk} \gamma^{mn} \kappa_{jma} \kappa_{ikn} \\ & + \frac{1}{2} \kappa_{icd} \kappa_{0be} n_a \left(g^{cb} g^{de} + \frac{1}{2} g^{be} n^c n^d \right) \\ & - \kappa_{icd} \kappa_{0ba} n^c \left(g^{bd} + \frac{1}{2} n^b n^d \right) \\ & + \frac{1}{2} \gamma_2 \left(n_a g^{cd} - 2\delta_a^c n^d \right) C_{icd}, \end{aligned} \quad (\text{A2})$$

and the time part is the lengthy expression

$$\begin{aligned} C_{0a} \equiv & -2n^b S_{ba} + n_a S_{bc} g^{bc} \\ & + \frac{1}{2} g_a^i g^{bc} \partial_i \kappa_{0bc} - \gamma^{ij} \partial_i \kappa_{0ja} - \gamma^{ij} n^b \partial_i \kappa_{jba} \\ & + \frac{1}{2} n_a g^{bc} \gamma^{ij} \partial_i \kappa_{jbc} + n_a \gamma^{ij} \partial_i H_j \\ & + g_a^i \kappa_{ijb} \gamma^{jk} \kappa_{kcd} \left(g^{bd} n^c - \frac{1}{2} g^{cd} n^b \right) \\ & - g_a^i n^b \partial_i H_b + \gamma^{ij} \kappa_{icd} \kappa_{jba} g^{bc} n^d \\ & - \frac{1}{2} n_a \gamma^{ij} \gamma^{mn} \kappa_{imc} \kappa_{njd} g^{cd} \\ & - \frac{1}{4} n_a \gamma^{ij} \kappa_{icd} \kappa_{jbe} g^{cb} g^{de} + \frac{1}{4} n_a \kappa_{0cd} \kappa_{0be} g^{cb} g^{de} \\ & - \gamma^{ij} H_i \kappa_{0ja} - n^b \gamma^{ij} \kappa_{0bi} \kappa_{0ja} \\ & - \frac{1}{4} g_a^i \kappa_{icd} n^c n^d \kappa_{0be} g^{be} + \frac{1}{2} n_a \kappa_{0cd} \kappa_{0be} g^{ce} n^d n^b \\ & + g_a^i \kappa_{icd} \kappa_{0be} n^c n^b g^{de} - \gamma^{ij} \kappa_{iba} n^b \kappa_{0je} n^e \\ & - \frac{1}{2} \gamma^{ij} \kappa_{icd} n^c n^d \kappa_{0ja} - \gamma^{ij} H_i \kappa_{jba} n^b \\ & + g_a^i \kappa_{icd} H_b g^{bc} n^d \\ & + \gamma_2 \left(\gamma^{id} C_{ida} - \frac{1}{2} g_a^i g^{cd} C_{icd} \right) \\ & + \frac{1}{2} n_a \kappa_{0cd} g^{cd} H_b n^b - n_a \gamma^{ij} \kappa_{ijc} H_d g^{cd} \\ & + \frac{1}{2} n_a \gamma^{ij} H_i \kappa_{jcd} g^{cd}. \end{aligned} \quad (\text{A3})$$

Perturbing Eq. (A2) to obtain the perturbation to the spatial part of the 2-index constraint, we find

$$\begin{aligned}
\Delta C_{ia} \equiv & \Delta \gamma^{jk} \partial_j \kappa_{ika} + \gamma^{jk} \partial_j \Delta \kappa_{ika} - \frac{1}{2} \Delta \gamma^j{}_a g^{cd} \partial_j \kappa_{icd} - \frac{1}{2} \gamma^j{}_a \Delta g^{cd} \partial_j \kappa_{icd} \\
& - \frac{1}{2} \gamma^j{}_a g^{cd} \partial_j \Delta \kappa_{icd} + \Delta n^b \partial_i \kappa_{0ba} + n^b \partial_i \Delta \kappa_{0ba} - \frac{1}{2} \Delta n_a g^{cd} \partial_i \kappa_{0cd} - \frac{1}{2} n_a \Delta g^{cd} \partial_i \kappa_{0cd} \\
& - \frac{1}{2} n_a g^{cd} \partial_i \Delta \kappa_{0cd} + \partial_i \Delta H_a + \frac{1}{2} \Delta g^j{}_a \kappa_{jcd} \kappa_{ief} g^{ce} g^{df} + \frac{1}{2} g^j{}_a \Delta \kappa_{jcd} \kappa_{ief} g^{ce} g^{df} \\
& + \frac{1}{2} g^j{}_a \kappa_{jcd} \Delta \kappa_{ief} g^{ce} g^{df} + \frac{1}{2} g^j{}_a \kappa_{jcd} \kappa_{ief} \Delta g^{ce} g^{df} + \frac{1}{2} g^j{}_a \kappa_{jcd} \kappa_{ief} g^{ce} \Delta g^{df} + \frac{1}{2} \Delta \gamma^{jk} \kappa_{jcd} \kappa_{ike} g^{cd} n^e n_a \\
& + \frac{1}{2} \gamma^{jk} \Delta \kappa_{jcd} \kappa_{ike} g^{cd} n^e n_a + \frac{1}{2} \gamma^{jk} \kappa_{jcd} \Delta \kappa_{ike} g^{cd} n^e n_a + \frac{1}{2} \gamma^{jk} \kappa_{jcd} \kappa_{ike} \Delta g^{cd} n^e n_a + \frac{1}{2} \gamma^{jk} \kappa_{jcd} \kappa_{ike} g^{cd} \Delta n^e n_a \\
& + \frac{1}{2} \gamma^{jk} \kappa_{jcd} \kappa_{ike} g^{cd} n^e \Delta n_a - \Delta \gamma^{jk} \gamma^{mn} \kappa_{jma} \kappa_{ikn} - \gamma^{jk} \Delta \gamma^{mn} \kappa_{jma} \kappa_{ikn} - \gamma^{jk} \gamma^{mn} \Delta \kappa_{jma} \kappa_{ikn} - \gamma^{jk} \gamma^{mn} \kappa_{jma} \Delta \kappa_{ikn} \\
& + \frac{1}{2} (\Delta \kappa_{icd} \kappa_{0be} n_a + \kappa_{icd} \Delta \kappa_{0be} n_a + \kappa_{icd} \kappa_{0be} \Delta n_a) \times \left(g^{cb} g^{de} + \frac{1}{2} g^{be} n^c n^d \right) \\
& + \frac{1}{2} \kappa_{icd} \kappa_{0be} n_a \left(\Delta g^{cb} g^{de} + g^{cb} \Delta g^{de} + \frac{1}{2} (\Delta g^{be} n^c n^d + g^{be} \Delta n^c n^d + g^{be} n^c \Delta n^d) \right) \\
& - (\Delta \kappa_{icd} \kappa_{0ba} n^c + \kappa_{icd} \Delta \kappa_{0ba} n^c + \kappa_{icd} \kappa_{0ba} \Delta n^c) \times \left(g^{bd} + \frac{1}{2} n^b n^d \right) \\
& - \kappa_{icd} \kappa_{0ba} n^c \left(\Delta g^{bd} + \frac{1}{2} \Delta n^b n^d + \frac{1}{2} n^b \Delta n^d \right) \\
& + \frac{1}{2} \gamma_2 \left(\Delta n_a g^{cd} + n_a \Delta g^{cd} - 2 \delta_a^c \Delta n^d \right) C_{icd} + \frac{1}{2} \gamma_2 \left(n_a g^{cd} - 2 \delta_a^c n^d \right) \Delta C_{icd},
\end{aligned} \tag{A4}$$

where ΔC_{icd} is the perturbed 3-index constraint as defined in Eq. (59).

Finally, the perturbation to the time part of the 2-index constraint is

$$\begin{aligned}
\Delta C_{0a} \equiv & -2\Delta n^b S_{ba} - 2n^b \Delta S_{ba} + \Delta n_a S_{bc} g^{bc} + n_a \Delta S_{bc} g^{bc} + n_a S_{bc} \Delta g^{bc} \\
& + \frac{1}{2} \left(\Delta g_a^i g^{bc} \partial_i \kappa_{0bc} + g_a^i \Delta g^{bc} \partial_i \kappa_{0bc} + g_a^i g^{bc} \partial_i \Delta \right) \kappa_{0bc} - \Delta \gamma^{ij} \partial_i \kappa_{0ja} - \gamma^{ij} \partial_i \Delta \kappa_{0ja} \\
& - \Delta \gamma^{ij} n^b \partial_i \kappa_{jba} - \gamma^{ij} \Delta n^b \partial_i \kappa_{jba} - \gamma^{ij} n^b \partial_i \Delta \kappa_{jba} \\
& + \frac{1}{2} \left(\Delta n_a g^{bc} \gamma^{ij} \partial_i \kappa_{jbc} + n_a \Delta g^{bc} \gamma^{ij} \partial_i \kappa_{jbc} + n_a g^{bc} \Delta \gamma^{ij} \partial_i \kappa_{jbc} + n_a g^{bc} \gamma^{ij} \partial_i \Delta \kappa_{jbc} \right) \\
& + \Delta n_a \gamma^{ij} \partial_i H_j + n_a \Delta \gamma^{ij} \partial_i H_j + n_a \gamma^{ij} \partial_i \Delta H_j \\
& + \left(\Delta g_a^i \kappa_{ijb} \gamma^{jk} \kappa_{kcd} + g_a^i \Delta \kappa_{ijb} \gamma^{jk} \kappa_{kcd} + g_a^i \kappa_{ijb} \Delta \gamma^{jk} \kappa_{kcd} + g_a^i \kappa_{ijb} \gamma^{jk} \Delta \kappa_{kcd} \right) \times \left(g^{bd} n^c - \frac{1}{2} g^{cd} n^b \right) \\
& + g_a^i \kappa_{ijb} \gamma^{jk} \kappa_{kcd} \left(\Delta g^{bd} n^c + g^{bd} \Delta n^c - \frac{1}{2} \Delta g^{cd} n^b - \frac{1}{2} g^{cd} \Delta n^b \right) \\
& - \Delta g_a^i n^b \partial_i H_b - g_a^i \Delta n^b \partial_i H_b - g_a^i n^b \partial_i \Delta H_b \\
& + \Delta \gamma^{ij} \kappa_{icd} \kappa_{jba} g^{bc} n^d + \gamma^{ij} \Delta \kappa_{icd} \kappa_{jba} g^{bc} n^d + \gamma^{ij} \kappa_{icd} \Delta \kappa_{jba} g^{bc} n^d + \gamma^{ij} \kappa_{icd} \kappa_{jba} \Delta g^{bc} n^d + \gamma^{ij} \kappa_{icd} \kappa_{jba} g^{bc} \Delta n^d \\
& - \frac{1}{2} \left(\Delta n_a \gamma^{ij} \gamma^{mn} \kappa_{imc} \kappa_{njd} g^{cd} + n_a \Delta \gamma^{ij} \gamma^{mn} \kappa_{imc} \kappa_{njd} g^{cd} + n_a \gamma^{ij} \Delta \gamma^{mn} \kappa_{imc} \kappa_{njd} g^{cd} \right. \\
& \quad \left. + n_a \gamma^{ij} \gamma^{mn} \Delta \kappa_{imc} \kappa_{njd} g^{cd} + n_a \gamma^{ij} \gamma^{mn} \kappa_{imc} \Delta \kappa_{njd} g^{cd} + n_a \gamma^{ij} \gamma^{mn} \kappa_{imc} \kappa_{njd} \Delta g^{cd} \right) \\
& - \frac{1}{4} \left(\Delta n_a \gamma^{ij} \kappa_{icd} \kappa_{jbe} g^{cb} g^{de} + n_a \Delta \gamma^{ij} \kappa_{icd} \kappa_{jbe} g^{cb} g^{de} + n_a \gamma^{ij} \Delta \kappa_{icd} \kappa_{jbe} g^{cb} g^{de} \right. \\
& \quad \left. + n_a \gamma^{ij} \kappa_{icd} \Delta \kappa_{jbe} g^{cb} g^{de} + n_a \gamma^{ij} \kappa_{icd} \kappa_{jbe} \Delta g^{cb} g^{de} + n_a \gamma^{ij} \kappa_{icd} \kappa_{jbe} g^{cb} \Delta g^{de} \right) \\
& + \frac{1}{4} \left(\Delta n_a \kappa_{0cd} \kappa_{0be} g^{cb} g^{de} + n_a \Delta \kappa_{0cd} \kappa_{0be} g^{cb} g^{de} + n_a \kappa_{0cd} \Delta \kappa_{0be} g^{cb} g^{de} + n_a \kappa_{0cd} \kappa_{0be} \Delta g^{cb} g^{de} + n_a \kappa_{0cd} \kappa_{0be} g^{cb} \Delta g^{de} \right) \\
& - \Delta \gamma^{ij} H_i \kappa_{0ja} - \gamma^{ij} \Delta H_i \kappa_{0ja} - \gamma^{ij} H_i \Delta \kappa_{0ja} - \Delta n^b \gamma^{ij} \kappa_{0bi} \kappa_{0ja} - n^b \Delta \gamma^{ij} \kappa_{0bi} \kappa_{0ja} - n^b \gamma^{ij} \Delta \kappa_{0bi} \kappa_{0ja} - n^b \gamma^{ij} \kappa_{0bi} \Delta \kappa_{0ja} \\
& - \frac{1}{4} \left(\Delta g_a^i \kappa_{icd} n^c n^d \kappa_{0be} g^{be} + g_a^i \Delta \kappa_{icd} n^c n^d \kappa_{0be} g^{be} + g_a^i \kappa_{icd} \Delta n^c n^d \kappa_{0be} g^{be} + g_a^i \kappa_{icd} n^c n^d \Delta \kappa_{0be} g^{be} \right. \\
& \quad \left. + g_a^i \kappa_{icd} n^c n^d \Delta \kappa_{0be} g^{be} + g_a^i \kappa_{icd} n^c n^d \kappa_{0be} \Delta g^{be} \right) + \frac{1}{2} \left(\Delta n_a \kappa_{0cd} \kappa_{0be} g^{ce} n^d n^b + n_a \Delta \kappa_{0cd} \kappa_{0be} g^{ce} n^d n^b \right. \\
& \quad \left. + n_a \kappa_{0cd} \Delta \kappa_{0be} g^{ce} n^d n^b + n_a \kappa_{0cd} \kappa_{0be} \Delta g^{ce} n^d n^b + n_a \kappa_{0cd} \kappa_{0be} g^{ce} \Delta n^d n^b + n_a \kappa_{0cd} \kappa_{0be} g^{ce} n^d \Delta n^b \right) \\
& + \Delta g_a^i \kappa_{icd} \kappa_{0be} n^c n^b g^{de} + g_a^i \Delta \kappa_{icd} \kappa_{0be} n^c n^b g^{de} + g_a^i \kappa_{icd} \Delta \kappa_{0be} n^c n^b g^{de} + g_a^i \kappa_{icd} \kappa_{0be} \Delta n^c n^b g^{de} \\
& + g_a^i \kappa_{icd} \kappa_{0be} n^c \Delta n^b g^{de} + g_a^i \kappa_{icd} \kappa_{0be} n^c n^b \Delta g^{de} - \Delta \gamma^{ij} \kappa_{iba} n^b \kappa_{0je} n^e - \gamma^{ij} \Delta \kappa_{iba} n^b \kappa_{0je} n^e - \gamma^{ij} \kappa_{iba} \Delta n^b \kappa_{0je} n^e \\
& - \gamma^{ij} \kappa_{iba} n^b \Delta \kappa_{0je} n^e - \gamma^{ij} \kappa_{iba} n^b \kappa_{0je} \Delta n^e - \frac{1}{2} \left(\Delta \gamma^{ij} \kappa_{icd} n^c n^d \kappa_{0ja} + \gamma^{ij} \Delta \kappa_{icd} n^c n^d \kappa_{0ja} + \gamma^{ij} \kappa_{icd} \Delta n^c n^d \kappa_{0ja} \right. \\
& \quad \left. + \gamma^{ij} \kappa_{icd} n^c \Delta n^d \kappa_{0ja} + \gamma^{ij} \kappa_{icd} n^c n^d \kappa_{0ja} + \gamma^{ij} \kappa_{icd} n^c n^d \Delta \kappa_{0ja} \right) \\
& - \Delta \gamma^{ij} H_i \kappa_{jba} n^b - \gamma^{ij} \Delta H_i \kappa_{jba} n^b - \gamma^{ij} H_i \Delta \kappa_{jba} n^b - \gamma^{ij} H_i \kappa_{jba} \Delta n^b + \Delta g_a^i \kappa_{icd} H_b g^{bc} n^d + g_a^i \Delta \kappa_{icd} H_b g^{bc} n^d \\
& + g_a^i \kappa_{icd} \Delta H_b g^{bc} n^d + g_a^i \kappa_{icd} H_b \Delta g^{bc} n^d + g_a^i \kappa_{icd} H_b g^{bc} \Delta n^d \\
& + \gamma_2 \left(\Delta \gamma^{id} C_{ida} + \gamma^{id} \Delta C_{ida} - \frac{1}{2} \left(\Delta g_a^i g^{cd} C_{icd} + g_a^i \Delta g^{cd} C_{icd} + g_a^i g^{cd} \Delta C_{icd} \right) \right) \\
& + \frac{1}{2} \left(\Delta n_a \kappa_{0cd} g^{cd} H_b n^b + n_a \Delta \kappa_{0cd} g^{cd} H_b n^b + n_a \kappa_{0cd} \Delta g^{cd} H_b n^b + n_a \kappa_{0cd} g^{cd} \Delta H_b n^b + n_a \kappa_{0cd} g^{cd} H_b \Delta n^b \right) \\
& - \Delta n_a \gamma^{ij} \kappa_{ijc} H_d g^{cd} - n_a \Delta \gamma^{ij} \kappa_{ijc} H_d g^{cd} - n_a \gamma^{ij} \Delta \kappa_{ijc} H_d g^{cd} - n_a \gamma^{ij} \kappa_{ijc} \Delta H_d g^{cd} - n_a \gamma^{ij} \kappa_{ijc} H_d \Delta g^{cd} \\
& + \frac{1}{2} \left(\Delta n_a \gamma^{ij} H_i \kappa_{jcd} g^{cd} + n_a \Delta \gamma^{ij} H_i \kappa_{jcd} g^{cd} + n_a \gamma^{ij} \Delta H_i \kappa_{jcd} g^{cd} + n_a \gamma^{ij} H_i \Delta \kappa_{jcd} g^{cd} + n_a \gamma^{ij} H_i \kappa_{jcd} \Delta g^{cd} \right),
\end{aligned}
\tag{A5}$$

where ΔS_{ab} is the perturbation to the source term as given by Eq. (50). We combine Eqs. (A4) and (A5) into one overall constraint,

$$\Delta C_{ab} = (\Delta C_{0a}, \Delta C_{ia}). \tag{A6}$$

Appendix B: Code tests

In order to have confidence in our dCS metric perturbation evolution results, we perform a suite of tests to check the accuracy of our metric perturbation evolution code. For each test, we check the convergence of the perturbed constraints derived in Sec. III E. Note that the results of

these tests do not contain new physics, but rather serve as a check of our implementation of the metric perturbation evolution equations (Eqs. (25), (26), and (27)).

1. Multipolar wave evolution

We first evolve a multipolar wave in the transverse-traceless gauge on a flat background [34, 35]. This evolution takes place on a domain with only one (outer) boundary, where we set the boundary condition given in Eq. (74). We wish to test the numerical evolution against the analytic solution. However, some of the terms in the evolution equations we are testing will vanish because the analytic solution has symmetries. To remove these symmetries, we perform a coordinate transformation of the form

$$r \rightarrow a\bar{r} + (a_0 - a)\frac{\bar{r}^3}{R^2}, \quad (\text{B1})$$

where $r \equiv \sqrt{x^2 + y^2 + z^2}$ in Cartesian grid coordinates, R and a_0 are constants, and $a(t)$ is a (time-dependent) function. We add an additional coordinate translation of the form

$$\bar{x}^i \rightarrow \bar{x}^i + C^i, \quad (\text{B2})$$

for some vector C^i .

We evolve an outgoing $l = 2, m = 2$ multipolar wave. This has a Gaussian profile, with an initial width of $1 M$, amplitude of 0.01 , and center of $10 M$. For the transformations given in Eqs. (B1) and (B2), we choose $R = 40 M$, $a_0 = 1.3$, $a(t) = 1 + 0.001t^2/M^2$ and $C^i = (2.0, -4.0, 3.0) M$. We evolve on a grid of nested spherical shells around a filled sphere, with an outer boundary of $R = 35 M$. Each shell has 8 radial spectral basis functions and 4 angular spectral basis functions at the lowest resolution, with 4 more basis functions added in each direction as we increase resolution. We find that the perturbed constraints, shown in Fig. 9, converge exponentially, and that the perturbed variables shown in Fig. 10 evolve toward zero (as the data leaves the domain) in a convergent way. Additionally, we check that our results converge to the known analytic solution.

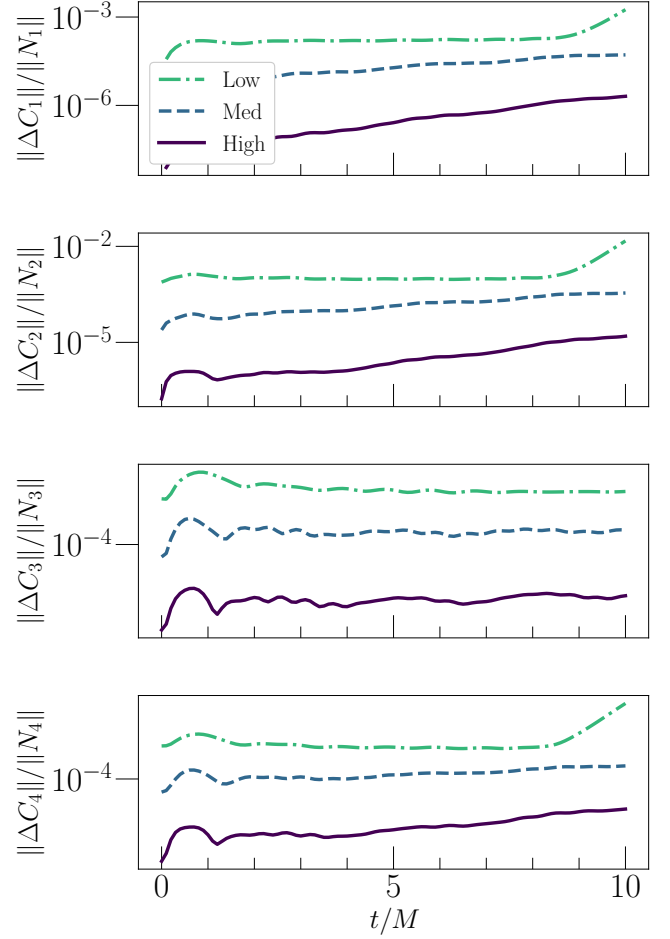


FIG. 9. Constraints for evolution of a transformed multipolar wave perturbation on flat space, as described in Sec. B1. For each constraint ΔC_A , we compute the L2 norm of the constraint over the entire computational domain ($\|\Delta C_1\|$ for the 1-index constraint, for example), and divide by the L2 norm of its normalization factor ($\|N_A\|$) (cf. Sec. III E). We see that the constraints converge exponentially with numerical resolution.

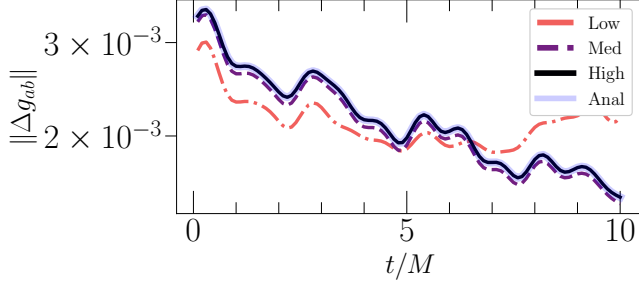


FIG. 10. Behavior of Δg_{ab} for the multipolar wave test described in Sec. B 1 for low, medium, and high resolution. We see that the value of the metric perturbation decreases as the wave propagates toward $R \rightarrow \infty$ (and leaves the computational domain), and that with increasing resolution the behavior of the variables converges to the highest-resolution value. We additionally plot the analytical solution for the behavior of the multipolar wave, which sits on top of the highest-resolution result.

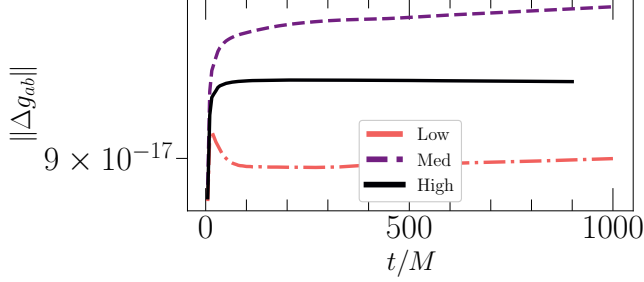


FIG. 11. Behavior of Δg_{ab} for the small data on Schwarzschild test described in Sec. B 2. We see that with increasing time, the field with initial magnitude of $\sim 10^{-16}$ remains close to roundoff error.

2. Small data on Schwarzschild

We perform a test where we initially set each component of Δg_{ab} to be a different number close to machine precision (10^{-16}) at each point on the domain, thus seeding any instabilities that might be present. We apply filtering to the spectral scheme in order to minimize the growth of high-frequency modes [27], and choose damping parameters γ_0 and γ_2 to be larger close to the horizon. We check that as the evolution progresses, the constraints and the values of Δg_{ab} and $\Delta \kappa_{abc}$ remain close to numerical truncation error. This in particular tests the constraint-damping capabilities of the code. We show the behavior of the perturbed variables in Fig. 11. We see that the solution remains at roundoff level. There is linear growth in Δg_{ab} , but the level of this growth decreases towards zero with increasing resolution.

-
- [1] C. M. Will, *Living Rev. Rel.* **17**, 4 (2014), [arXiv:1403.7377 \[gr-qc\]](#).
 - [2] B. P. Abbott *et al.* (Virgo, LIGO Scientific), *Phys. Rev. Lett.* **116**, 221101 (2016), [Erratum: *Phys. Rev. Lett.* 121, no. 12, 129902 (2018)], [arXiv:1602.03841 \[gr-qc\]](#).
 - [3] N. Yunes, K. Yagi, and F. Pretorius, *Phys. Rev.* **D94**, 084002 (2016), [arXiv:1603.08955 \[gr-qc\]](#).
 - [4] S. Alexander and N. Yunes, *Phys. Rept.* **480**, 1 (2009), [arXiv:0907.2562 \[hep-th\]](#).
 - [5] M. B. Green and J. H. Schwarz, *Phys. Lett.* **149B**, 117 (1984).
 - [6] V. Taveras and N. Yunes, *Phys. Rev.* **D78**, 064070 (2008), [arXiv:0807.2652 \[gr-qc\]](#).
 - [7] S. Mercuri and V. Taveras, *Phys. Rev.* **D80**, 104007 (2009), [arXiv:0903.4407 \[gr-qc\]](#).
 - [8] S. Weinberg, *Phys. Rev.* **D77**, 123541 (2008), [arXiv:0804.4291 \[hep-th\]](#).
 - [9] T. Delsate, D. Hilditch, and H. Witek, *Phys. Rev.* **D91**, 024027 (2015), [arXiv:1407.6727 \[gr-qc\]](#).
 - [10] M. Okounkova, L. C. Stein, M. A. Scheel, and D. A. Hemberger, *Phys. Rev.* **D96**, 044020 (2017), [arXiv:1705.07924 \[gr-qc\]](#).
 - [11] C. Molina, P. Pani, V. Cardoso, and L. Gualtieri, *Phys. Rev.* **D81**, 124021 (2010), [arXiv:1004.4007 \[gr-qc\]](#).
 - [12] D. Garfinkle, F. Pretorius, and N. Yunes, *Phys. Rev.* **D82**, 041501 (2010), [arXiv:1007.2429 \[gr-qc\]](#).
 - [13] E. Berti *et al.*, *Class. Quant. Grav.* **32**, 243001 (2015), [arXiv:1501.07274 \[gr-qc\]](#).
 - [14] T. W. Baumgarte and S. L. Shapiro, *Numerical Relativity: Solving Einstein's Equations on the Computer* (Cambridge University Press, Cambridge, England, 2010).
 - [15] M. Okounkova, M. A. Scheel, and S. A. Teukolsky, (2018), submitted to *Class. Quant. Grav.*, [1810.05306](#).
 - [16] L. Lindblom, M. A. Scheel, L. E. Kidder, R. Owen, and O. Rinne, *Class. Quant. Grav.* **23**, S447 (2006), [arXiv:gr-qc/0512093 \[gr-qc\]](#).
 - [17] H. Friedrich, *Comm. Math. Phys.* **100**, 525 (1985).
 - [18] F. Pretorius, *Class. Quant. Grav.* **22**, 425 (2005), [arXiv:gr-qc/0407110 \[gr-qc\]](#).
 - [19] F. Pretorius, *Phys. Rev. Lett.* **95**, 121101 (2005), [arXiv:gr-qc/0507014 \[gr-qc\]](#).
 - [20] M. A. Scheel, M. Boyle, T. Chu, L. E. Kidder, K. D. Matthews, and H. P. Pfeiffer, *Phys. Rev.* **D79**, 024003 (2009), [arXiv:0810.1767 \[gr-qc\]](#).
 - [21] “The Spectral Einstein Code (SpEC),” <http://www.black-holes.org/SpEC.html>.
 - [22] L. E. Kidder, L. Lindblom, M. A. Scheel, L. T. Buchman, and H. P. Pfeiffer, *Phys. Rev.* **D71**, 064020 (2005), [arXiv:gr-qc/0412116 \[gr-qc\]](#).
 - [23] O. Rinne, L. Lindblom, and M. A. Scheel, *Class. Quant. Grav.* **24**, 4053 (2007), [arXiv:0704.0782 \[gr-qc\]](#).
 - [24] O. Rinne, L. T. Buchman, M. A. Scheel, and H. P. Pfeiffer, *Class. Quant. Grav.* **26**, 075009 (2009), [arXiv:0811.3593 \[gr-qc\]](#).
 - [25] D. A. Hemberger, M. A. Scheel, L. E. Kidder, B. Szilágyi, G. Lovelace, N. W. Taylor, and S. A. Teukolsky, *Class. Quant. Grav.* **30**, 115001 (2013), [arXiv:1211.6079 \[gr-qc\]](#).
 - [26] L. C. Stein, *Phys. Rev.* **D90**, 044061 (2014), [arXiv:1407.2350 \[gr-qc\]](#).
 - [27] B. Szilágyi, L. Lindblom, and M. A. Scheel, *Phys. Rev.* **D80**, 124010 (2009), [arXiv:0909.3557 \[gr-qc\]](#).
 - [28] N. Yunes and F. Pretorius, *Phys. Rev.* **D79**, 084043 (2009), [arXiv:0902.4669 \[gr-qc\]](#).
 - [29] K. Konno, T. Matsuyama, and S. Tanda, *Prog. Theor. Phys.* **122**, 561 (2009), [arXiv:0902.4767 \[gr-qc\]](#).
 - [30] D. Ayzenberg and N. Yunes, (2018), [arXiv:1807.08422 \[gr-qc\]](#).
 - [31] A. H. Mroue *et al.*, *Phys. Rev. Lett.* **111**, 241104 (2013), [arXiv:1304.6077 \[gr-qc\]](#).
 - [32] G. Lovelace, *Class. Quant. Grav.* **26**, 114002 (2009).
 - [33] B. Szilágyi, *Int. J. Mod. Phys.* **D23**, 1430014 (2014), [arXiv:1405.3693 \[gr-qc\]](#).
 - [34] S. A. Teukolsky, *Phys. Rev. D* **26**, 745 (1982).
 - [35] O. Rinne, *Class. Quant. Grav.* **26**, 048003 (2009), [arXiv:0809.1761 \[gr-qc\]](#).